GRB 191019A

Lazzati, Davide; Perna, Rosalba; Gompertz, Benjamin P.; Levan, Andrew J.

DOI:
10.3847/2041-8213/acd18c

Document Version
Publisher's PDF, also known as Version of record

Citation for published version (Harvard):
Lazzati, D, Perna, R, Gompertz, BP & Levan, AJ 2023, 'GRB 191019A: A Short Gamma-Ray Burst in Disguise from the Disk of an Active Galactic Nucleus', *Astrophysical Journal Letters*, vol. 950, no. 2, L20. https://doi.org/10.3847/2041-8213/acd18c

The Astrophysical Journal Letters, 950:L20 (6pp), 2023 June 20 https://doi.org/10.3847/2041-8213/acd18c

GRB 191019A: A Short Gamma-Ray Burst in Disguise from the Disk of an Active Galactic Nucleus

Davide Lazzati[1], Rosalba Perna[2,3], Benjamin P. Gompertz[4], and Andrew J. Levan[5,6]
[1] Department of Physics, Oregon State University, 301 Weniger Hall, Corvallis, OR 97331, USA; lazzatid@science.oregonstate.edu
[2] Department of Physics and Astronomy, Stony Brook University, Stony Brook, NY 11794-3800, USA
[3] Center for Computational Astrophysics, Flatiron Institute, New York, NY 10010, USA
[4] School of Physics and Astronomy & Institute for Gravitational Wave Astronomy, University of Birmingham, Birmingham, B15 2TT, UK
[5] Department of Astrophysics/IMAPP, Radboud University Nmegen, P.O. Box 9010, 6500 GL Nmegen, The Netherlands
[6] Department of Physics, University of Warwick, Coventry, CV4 7AL, UK
Received 2023 March 22; revised 2023 April 20; accepted 2023 April 23; published 2023 June 22

Abstract

Long and short gamma-ray bursts (GRBs), canonically separated at around 2 s duration, are associated with different progenitors: the collapse of a massive star and the merger of two compact objects, respectively. GRB 191019A was a long GRB ($T_{90} \sim 64$ s). Despite the relatively small redshift $z = 0.248$ and Hubble Space Telescope follow-up observations, an accompanying supernova was not detected. In addition, the host galaxy did not have significant star formation activity. Here we propose that GRB 191019A was produced by a binary compact merger, whose prompt emission was stretched in time by the interaction with a dense external medium. This would be expected if the burst progenitor was located in the disk of an active galactic nucleus, as supported by the burst localization close to the center of its host galaxy. We show that the light curve of GRB 191019A can be well modeled by a burst of intrinsic duration $t_{\rm eng} = 1.1$ s and of energy $E_{\rm iso} = 10^{51}$ erg seen moderately off axis, exploding in a medium of density $\sim 10^7$–10^8 cm^{-3}. The double-peaked light curve carries the telltale features predicted for GRBs in high-density media, where the first peak is produced by the photosphere and the second by the overlap of reverse shocks that take place before the internal shocks could happen. This would make GRB 191019A the first confirmed stellar explosion from within an accretion disk, with important implications for the formation and evolution of stars in accretion flows and for gravitational-waves source populations.

Unified Astronomy Thesaurus concepts: Gamma-ray bursts (629); Galaxy accretion disks (562); Stellar evolution (1599)

1. Introduction

Long and short gamma-ray bursts (GRBs) have been traditionally associated with galactic environments, where ambient densities are generally small or moderate (few to hundreds of protons per cm^{-3}). However, the possibility that a fraction of them may originate in the disks of active galactic nuclei (AGNs) has been gaining some interest, especially in light of the fact that AGN disks have been shown to be a promising channel to explain some unexpected findings of the LIGO/Virgo data. These include black holes (BHs) both in the low- (Abbott et al. 2020a; Tagawa et al. 2020; Yang et al. 2020) and high-mass gaps (Abbott et al. 2020b), and evidence for asymmetry in the BH spin distribution (Callister et al. 2021; McKernan et al. 2022; Wang et al. 2021).

The presence of neutron stars (NSs) and BHs embedded in AGN disks is not surprising since they are the remnants of massive stars. Stars are expected to be present in these disks as a result of two processes: capture from the nuclear star cluster surrounding the AGN (e.g., Artymowicz et al. 1993) and in situ formation from gravitational instabilities in the outer disk (e.g., Goodman 2003; Dittmann & Miller 2020). Once formed or captured, stars in AGN disks follow different evolutionary paths compared to their galactic counterparts. The very large densities and strong torques of the AGN disk environments cause stars embedded in them to both grow to large masses (Cantiello et al. 2021; Dittmann et al. 2021) as well as to acquire angular speed (Jermyn et al. 2021), which makes them ideal candidates as progenitors of long GRBs.

Additionally, and especially important for our investigation, short GRBs are expected to explode in AGN disks. Short GRBs are known to be the result of a merger of two NSs (Abbott et al. 2017) and potentially also of an NS–BH merger for nonextreme mass ratios. NSs can be formed in AGN disks either in situ from the direct collapse of stars or as a result of capture from the nuclear star cluster (Tagawa et al. 2020; Perna et al. 2021b). Binary formation via dynamical interactions is then facilitated by gas drag (Tagawa et al. 2020) as well as by compact-object clustering in migration traps (e.g., Bellovary et al. 2016; McKernan et al. 2020).

The medium of an AGN disk, due to its high density, can, however, significantly change the appearance of a GRB. Depending on the disk size and location within the disk, GRBs can be choked (Zhu et al. 2021b) or appear diffused (Perna et al. 2021a; Wang et al. 2022). In some cases, they would also produce luminous neutrino bursts (Zhu et al. 2021a). Time-dependent photoionization of the intervening material up to the photosphere can further alter early-time emission (Ray et al. 2023). In addition, the high density of the medium can dramatically change the intrinsic spectra and light curves. Lazzati et al. (2022) showed that in high-density environments, GRBs are likely characterized by a single, long-emission episode that is due to the superposition of individual pulses, with a characteristic hard-to-soft evolution irrespective of the

light-curve luminosity. Short-duration GRBs can become long GRBs. Additionally, a distinctive feature would be the lack of an associated supernova component and a position coincident with the center of the host galaxy.

A burst with the key features of a GRB with a compact merger engine from an AGN disk has been recently identified (Levan et al. 2023) in GRB 191019A, as described in the Section 2. Here, using our formalism for the computation of the light curve of GRBs in very dense media (Lazzati et al. 2022), we model the light curve of GRB 191019A and derive the properties of its engine, as well as the density of the medium, which we find consistent with that of an AGN disk.

The paper is organized as follows: Section 2 describes the observations of GRB 191019A; our numerical methods for the light curve modeling are described in Section 3. The simulation results are presented in Section 4, and we summarize and put our results in context in Section 5.

2. GRB 191019A

GRB 191019A was detected by the Neil Gehrels Swift Observatory on 2019 October 19. Its duration of $T_{90} = 64.4 \pm 4.5$ s indicated its belonging to the class of long GRBs. The light curve was characterized by a fast rise and an exponential decay (a.k.a. FRED), with some evidence of hard-to-soft spectral evolution and overlaid variability. Optical observations with the Nordic Optical Telescope revealed a faint optical transient whose location was pinpointed within $\sim$100 pc of the nucleus of its host galaxy, whose redshift was measured to be $z = 0.248$ (Levan et al. 2023).

Despite the relatively low redshift of the burst and deep follow-up observations with the Hubble Space Telescope, no supernova counterpart was identified, making its classification as a long GRB questionable. Additionally, the lack of evidence for star formation in the host galaxy cast further doubt on its origin from the collapse of a massive star. Levan et al. (2023) suggested that GRB 191019A is rather the result of the merger of two compact objects, involving white dwarfs, NSs, or BHs, and that dynamical interactions in the dense cluster surrounding the central supermassive black hole of the host galaxy are responsible for forming the binary that eventually merged.

Our interpretation is broadly consistent with theirs in that we consider that GRB 191019A is rather the result of a binary merger than a collapsar, and that it originated in an environment prone to binary formation via dynamical interactions. However, we make our suggestion more specific by proposing that GRB 191019A is a rather typical short GRB emerging from the disk of an AGN, and, as shown in the following, we support it by demonstrating that its light curve and spectral evolution can be modeled as that of a short GRB exploding in a high-density medium.

3. Methods

We model the light curve of the prompt emission of GRB 191019A based on the model developed in Lazzati et al. (2022). To improve on their original setup, we also consider the emission from the fireball's photosphere. In this section, we describe in detail the model for the photospheric component and briefly summarize the Lazzati et al. (2022) model for the synchrotron shock component.

Photospheric emission in GRB fireballs has been extensively studied, both analytically (Pe'er et al. 2005; Giannios 2006; Pe'er et al. 2006; Giannios & Spruit 2007) and numerically (Chhotray & Lazzati 2015; Ito et al. 2015; Lazzati 2016; Parsotan & Lazzati 2018; Ito et al. 2021). Let us consider a fireball that is launched through a nozzle at a radius r_0 with bulk Lorentz factor $\Gamma_0 = 1$ and isotropic luminosity $L_{\rm iso}$. Its nozzle temperature is

$$T_0 = \left(\frac{L_{\rm iso}}{4\pi r_0^2 ac}\right)^{\frac{1}{4}}, \tag{1}$$

where $a = 7.56 \times 10^{-15}$ erg cm^{-3} K^{-4} is the radiation density constant. The temperature decreases with distance due to the fireball's acceleration. At the saturation radius $r_{\rm sat}$, where the fireball ends its acceleration, it has reached a value

$$T_{\rm sat} = \frac{T_0}{\eta}, \tag{2}$$

where $\eta = L_{\rm iso}/(\dot{m}c^2)$ is the fireball's asymptotic Lorentz factor. Beyond saturation, the temperature drops adiabatically until the photospheric radius is reached, at which point the advected radiation is released to form the photospheric component of the prompt light curve. The temperature at the photospheric radius therefore reads (e.g., Piran 2004):

$$T_{\rm ph} = T_{\rm sat}\left(\frac{r_{\rm ph}}{r_{\rm sat}}\right)^{-\frac{2}{3}} = \frac{T_0}{\eta}\left(\frac{r_{\rm ph}}{r_{\rm sat}}\right)^{-\frac{2}{3}}. \tag{3}$$

The above equation gives the fireball temperature at the stage in which the radiation is released. Because of the blueshift due to the bulk motion toward the observer, the observed color temperature of the radiation is

$$T_{\rm obs} = \eta T_{\rm ph} = T_0\left(\frac{r_{\rm ph}}{r_{\rm sat}}\right)^{-\frac{2}{3}}, \tag{4}$$

which depends only on the fireball's initial conditions through T_0 and on the two characteristic radii $r_{\rm sat}$ and $r_{\rm ph}$. For the latter, we use Equation (6) from Lazzati et al. (2020), which includes both thin and thick fireballs and incorporates the possibility of an electron fraction $Y_e \leqslant 1$. The smaller the electron fraction, the lower the Thomson thickness of the fireball and the sooner the photospheric component is released, causing an earlier and hotter photospheric component.

To calculate $r_{\rm sat}$ we follow the standard fireball model (Piran 2004), but we introduce a parameter $\alpha_{\rm acc}$ that controls the efficiency of the acceleration. In a standard fireball, evolving in vacuum, the fireball is spherical or conical (if beamed), and the acceleration is linear with distance: $\Gamma(r) = r/r_0$. Theoretical considerations (Matzner 2003; Bromberg & Levinson 2007; Lazzati & Perna 2019; Gottlieb & Nakar 2022) and numerical simulations for both collapsars and binary NS mergers (MacFadyen & Woosley 1999; Aloy et al. 2000; Morsony et al. 2007; Murguia-Berthier et al. 2014; Nagakura et al. 2014; Gottlieb et al. 2021) have, however, shown that a jet expanding in an external medium is shocked and hydrodynamically collimated. This nonconical evolution delays acceleration, causing the saturation radius to happen at a greater distance, therefore reducing the length scale over which adiabatic cooling takes place, and eventually causing a brighter and hotter photosphere. We parameterize this deviation from conical evolution through a parameter $\alpha_{\rm acc}$ that is intrinsically

defined through

$$\Gamma(r) = \left(\frac{r}{r_0}\right)^{\alpha_{\rm acc}}, \tag{5}$$

which modifies the equation for the saturation radius as

$$r_{\rm sat} = r_0\, \eta^{\frac{1}{\alpha_{\rm acc}}}. \tag{6}$$

Putting it all together, we arrive at the equations for the observed energetics of the photospheric emission, its observed peak frequency, and the observed duration of the pulse. The comoving energetics is given by the blackbody radiation density times the fireball volume, which is boosted by η^2 to calculate the observed isotropic equivalent energy:

$$E_{\rm ph,iso} = 4\pi r_{\rm ph}^2 c t_{\rm eng} a T_{\rm ph}^4 \eta^2, \tag{7}$$

where $t_{\rm eng}$ is the time the central engine is active. Using Equations (1), (3), and (6), we obtain

$$E_{\rm ph,iso} = L_{\rm iso}\left(\frac{r_0}{r_{\rm ph}}\right)^{\frac{2}{3}} \eta^{\frac{8-6\alpha_{\rm acc}}{3\alpha_{\rm acc}}} t_{\rm eng}. \tag{8}$$

Analogously, the peak photon energy in keV is obtained as

$$\begin{aligned} h\nu_{\rm pk} &= \frac{2.8}{1.6\times10^{-9}} k_B T_{\rm ph}\eta \\ &= 1.75\times10^{9} k_B \left(\frac{L}{4\pi a c}\right)^{\frac{1}{4}} \frac{r_0^{\frac{5}{12}}}{r_{\rm ph}^{\frac{2}{3}}} \eta^{\frac{2}{3\alpha_{\rm acc}}}, \end{aligned} \tag{9}$$

where k_B is the Boltzmann constant. Finally, the duration of the photospheric pulse is set either by the engine duration $t_{\rm eng}$ or by the curvature timescale, whichever is longer:

$$\Delta t_{\rm ph} = \max\left(t_{\rm eng}, \frac{r_{\rm ph}}{c\eta^2}\right). \tag{10}$$

Following the photospheric pulse is a train of pulses caused by the repeated shocking of the external medium caused by the incoming fireball shells. The unique feature of the model is that, due to the high external medium density, the external shocks take place very close to the central engine, at a distance that is smaller than the one at which internal shocks are expected. Lazzati et al. (2022) show that this causes a train of pulses whose duration is significantly longer than their spacing, creating a broad pulse with hard-to-soft spectral evolution. In the following, we model the prompt light curve of GRB 191019A as the superposition of the photospheric pulse discussed above and the train of shocks discussed in Lazzati et al. (2022).

The particular setup chosen for the modeling has a central engine with $t_{\rm eng}$ fixed at 1.1 s. The fireball is made of six 0.1 s pulses with identical properties separated by dead times of 0.1 s duration. Each pulse carries one-sixth of the overall energy (which is a fit parameter) and has an asymptotic Lorentz factor η (also a fit parameter). The nozzle radius r_0 is fixed at $r_0 = 10^8$ cm. The external medium is assumed to be uniform with density $n_{\rm ext}$ (a fit parameter). The microphysical parameters for computing the radiation efficiency are held fixed at $\varepsilon_e = 0.2$ and $\varepsilon_B = 0.01$. The electron fraction Y_e and the acceleration efficiency $\alpha_{\rm acc}$ are the two final fit parameters.

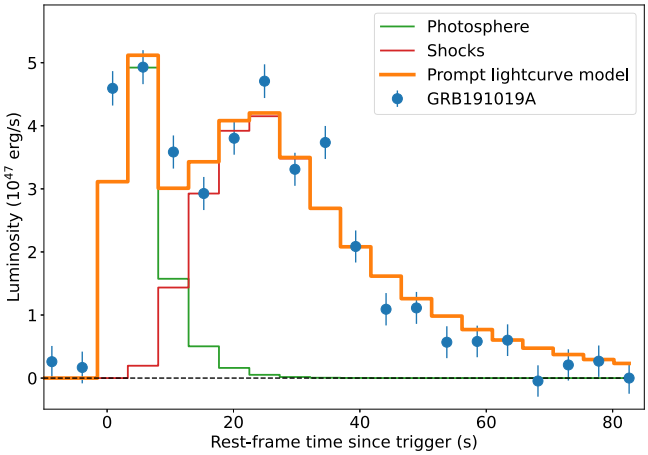

Figure 1. Best-fit model for the prompt light curve of GRB 191019A. Neil Gehrels Swift Observatory data (blue symbols) are adapted from Levan et al. (2023). The thick orange line shows the best-fit model for the overall prompt light curve. The thin green line marks the photospheric component, while the thin red line displays the contribution of the strong reverse shocks driven into the fireball by the dense external medium.

4. Modeling Results

As described in Section 3, the prompt light curve of GRB 191019A was modeled with five free parameters. We used the Monte Carlo Markov Chain implementation emcee (Foreman-Mackey et al. 2013) for minimizing the χ^2. Flat priors were assumed for the logarithm of the burst isotropic equivalent energy $E_{\rm iso}$, the fireball's asymptotic Lorentz factor η, the external medium density $n_{\rm ext}$, and the electron fraction Y_e. A flat prior in linear space was instead assumed for the acceleration efficiency $\alpha_{\rm acc}$. The best-fit light curve is shown in Figure 1 while the corner plot of parameter estimation with posterior uncertainties is shown in Figure 2.

The overall fit is acceptable, even if some deviations are noticeable (Figure 1). These are due to the fact that we are not attempting to carry out a formal fit to the data. The unknown properties of the GRB engine are too many. Investigating, e.g., whether the engine duration is different from 1.1 s or whether the number of shells ejected is truly six is beyond the scope of this paper. What we focus here is showing that a vanilla short GRB in terms of energy, engine duration, and Lorentz factor can reproduce the overall shape of the burst, and we can set limits on the properties of the external medium. In addition, we note that we have binned the prompt light curve from Levan et al. (2023) and may have smoothed out some short timescale variability in the process. Some variability on timescales shorter than the overall burst duration is expected in our model due to the fact that each shell from the engine produces a reverse shock with its individual peak time and duration. As discussed above, a detailed fit with individual shell ejection times, Lorentz factors, thicknesses, and energetics is beyond the scope of this paper. In addition, such a fit would not be supported by the low signal-to-noise ratio of the prompt light curve. We stress, however, that if well-separated peaks were present in the light curve, it would make it difficult to reconcile the data with the model.

As seen in Figure 2, a vanilla short GRB is indeed what is preferred by the data, with the exception of the asymptotic Lorentz factor η, which is found to be small, of order 10. While this is lower than the fiducial on-axis burst expectation

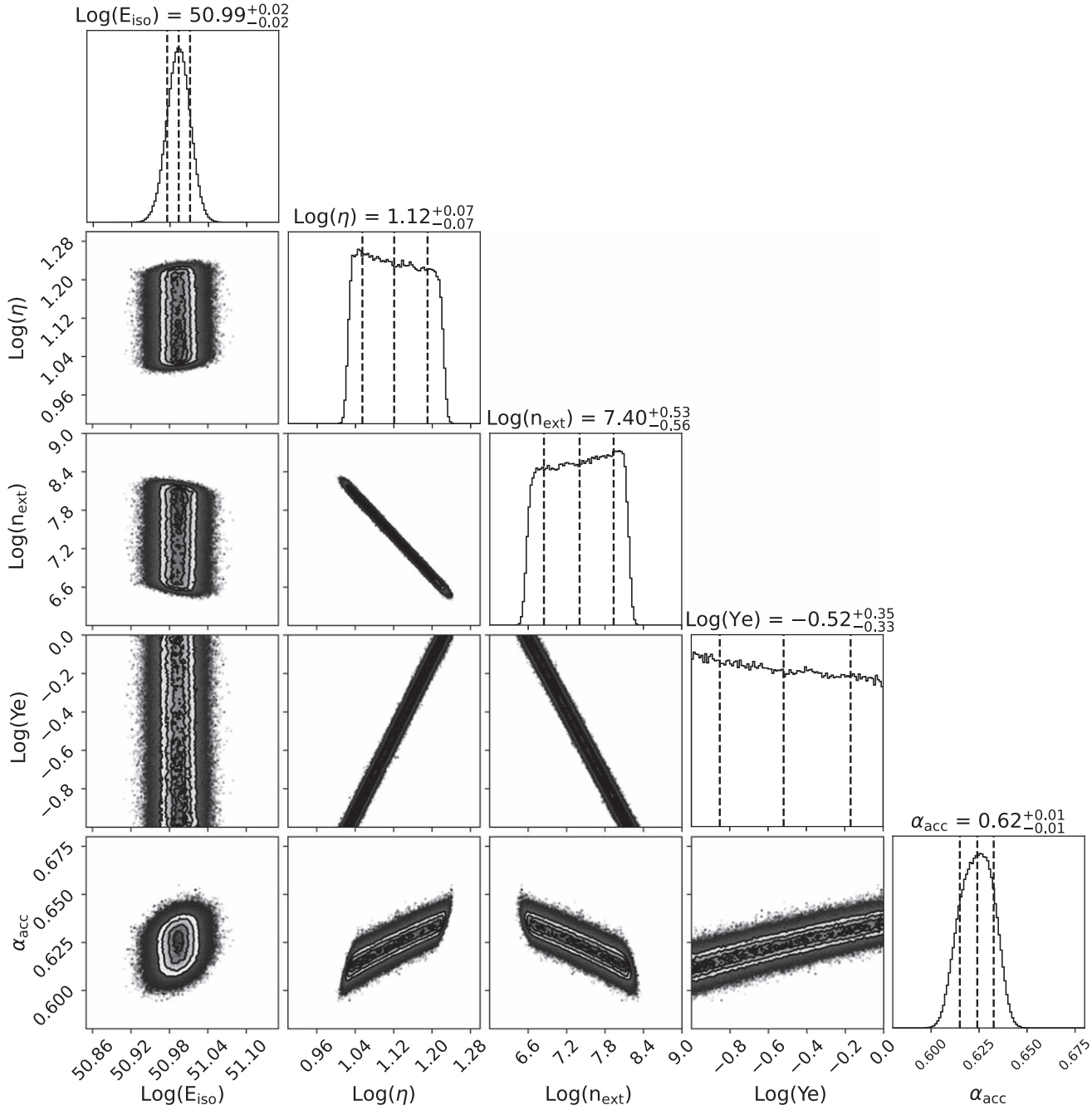

Figure 2. Monte Carlo Markov Chain parameter estimation for the prompt light curve of GRB 191019A. All parameters are well constrained, with the exception of the electron fraction Y_e, which only shows a mild preference for small values.

($\eta \sim 100$), it is not surprising. The asymptotic Lorentz factor is a function of the viewing angle and the likelihood of seeing a perfectly on-axis burst is vanishingly small. Comparing our inferred value with simulation results for the well-studied GW170817 (Lazzati et al. 2018; Salafia et al. 2020), we find that a viewing angle of $\sim 10^\circ$ is inferred.

Most interesting is the fairly tight constraint on the external density, which is found to be bound by $10^7\,\mathrm{cm}^{-3} \lesssim n_{\rm ext} \lesssim 10^8\,\mathrm{cm}^{-3}$, with a slight preference for the higher values. This is the highest density inferred for any burst to date. A closer inspection of Figure 2 reveals a tight correlation between external density, Lorentz factor, and electron fraction. Of the three, the electron fraction Y_e is not constrained by the data, which only show a marginal preference for low values over the range allowed by the flat prior. The acceleration efficiency is found to be fairly low, in keeping with numerical predictions of short GRB jets expanding in the dynamical ejecta of the binary (Murguia-Berthier et al. 2014; Nagakura et al. 2014; Lazzati et al. 2018).

The spectral information from the model was not used since the spectrum of GRB 191019A is consistent with a single steep power law, indicating that the peak frequency lies below the instrumental band or near its edge. We carried out an a posteriori check and found that our best model predicts a peak frequency of approximately 3 keV, consistent with the observational constraints.

5. Summary and Discussion

We have shown that GRB 191019A can be well modeled as a short GRB of intrinsic duration 1.1 s, isotropic energy $E_{\rm iso} = 10^{51}$ erg, and moderate Lorentz factor $\eta = 10$, emerging from a circumburst medium of density $n_{\rm ext} \sim 10^7$–10^8 cm^{-3}. This value is higher than even the densest known molecular clouds but fully consistent with the outer parts of an AGN disk.

The host galaxy of GRB 191019A has a smooth morphology with a very compact, almost point-like core. A scaling relation with the galaxy mass would imply a central SMBH of a few $\times 10^7 M_\odot$. Levan et al. (2023) explored the possibility that the central light concentration could arise from an AGN. The observation of a weak [N II] line combined with the absence of hydrogen or oxygen lines was found to be compatible with an AGN-like set of line ratios although this is not conclusive. Late observations with the Swift X-Ray Telescope set a limit on the X-ray luminosity of $L_{\rm X} < 6 \times 10^{42}$ erg s^{-1}, which rules out a high-luminosity AGN while still leaving the possibility of a low-luminosity one.[7] The localization of GRB 191019A within the innermost 100 pc of its host galaxy makes the AGN disk interpretation especially tantalizing. However, we note that, for this scenario to hold, either the SMBH mass has to be somewhat lower than the relatively high value implied by the galaxy mass, or accretion has to be somewhat lower than the close-to-Eddington rate typically assumed, to allow for both a low-luminosity AGN as well as a not-too-massive disk that would diffuse the GRB radiation (see discussion in Perna et al. 2021a).[8] In the following, to make our discussion more quantitative using specific examples from the literature, we will consider an AGN disk around an SMBH of $4 \times 10^6 M_\odot$.

In order to relate the inferred circumburst density to that of an AGN disk, we can refer to specific disk models that have been developed in the literature, in particular, the ones of Sirko & Goodman (2003) and of Thompson et al. (2005). A central density of $\sim 10^7$–10^8 cm^{-3} is realized between $\sim 5 \times 10^5$–10^6 gravitational radii (R_g) for the former model and $\sim (10^6$–$3 \times 10^6) R_g$ for the latter. For a $4 \times 10^6 M_\odot$ SMBH, the range of density inferred for the ambient medium of GRB 101019A would hence correspond to radial distances between a tenth of a pc to a pc.

It is interesting to compare these findings with results of numerical simulations of a population of NSs evolving in the specific environment of an AGN disk. Using the *N*-body code developed by Tagawa et al. (2020) for compact-object evolution in an AGN disk, Perna et al. (2021b) investigated the fate of the NS population. A generic finding of their modeling (i.e., independent of the model parameters) is that NS–NS mergers preferentially occur in two regions within the disk, one at very small radii and another at large radii. For their fiducial model with SMBH mass $4 \times 10^6\, M_\odot$, they found these two regions to be located at about $\sim 10^{-4}$–10^{-3} pc and $\sim$0.1–1 pc, respectively. The physical reason for this bimodal distribution lies in the fact that, below $\sim$0.1 pc, migration times are fast enough for the NSs to migrate toward the central disk regions within the AGN lifetime. On the other hand, NSs initially in the outer disk regions, where migration times are very long, will tend to remain in the same sites where they were either born or captured from the nuclear star cluster. Therefore, theoretical models predict a roughly bimodal NS–NS merger distribution (see Figure 2 in Perna et al. 2021b). It is especially intriguing that the density in the outer disk regions that we infer from the best-fit modeling to the light curve of GRB 191019A points to one of the two regions (namely, the outer one) from which NS–NS mergers are in fact expected with higher probability. In addition, these regions are also those in which the burst is expected to emerge from the disk without being diffused or significantly absorbed by the disk material (see Figure 5 in Perna et al. 2021a), consistent with the fact that the burst appearance is intrinsic within our model. While the disk has a significant column density for the considered scenario ($N_H \sim 10^{22}$ cm^{-2}, assuming a disk thickness $\sim$1% of the radius), the burst itself would destroy dust and photoionize the whole disk material, rendering any absorption undetectable (Ray et al. 2023). This is also consistent with GRB 191019A not showing significant absorption in its afterglow (Levan et al. 2023).

Our modeling implies a modest initial Lorentz factor $\eta \sim 10$, suggestive of a viewing angle $\sim 10^\circ$ (Lazzati et al. 2018; Salafia et al. 2020). The NS–NS binary is likely to have its orbital angular momentum aligned with that of the AGN disk (due to either birth within the disk itself or orbital alignment after capture from the nuclear star cluster),[9] unless a scattering with a tertiary perturbs its orbit (Samsing et al. 2022). The jet of a short GRB is in turn likely pointing in the direction of the orbital angular momentum (e.g., Ruiz et al. 2016). Therefore, our inferred viewing angle of 10° is likely indicating the inclination of the host disk with respect to the observer. The angular momentum of the disk is hence misaligned with respect to the angular momentum of the galaxy, which is seen nearly edge on (Levan et al. 2023). This is not surprising, given that observations of various kinds point to a near-complete lack of correlation between these two quantities (e.g., Kinney et al. 2000), and numerical simulations (e.g., Hopkins et al. 2012) further support such misalignment. Our interpretation and modeling of the event GRB 191019A hence lead to a novel way to measure the AGN disk/galaxy offset.

The only part of the data that we do not include in our model is the afterglow. GRB 191019A had an X-ray afterglow and a single detection in the optical (Levan et al. 2023). Given the burst redshift, the afterglow is weaker than average but not particularly unusual. A precise modeling of GRB afterglows in dense media is made difficult by the fact that the self-absorption frequency can exceed the injection frequency, possibly preventing the formation of a power-law distribution (Ghisellini et al. 1998). For these reasons, we only notice that a general prediction of a dimmer-than-average afterglow is consistent with the model characteristics (Lazzati et al. 2022), but we do not attempt a formal afterglow model. A future fit of the afterglow data when a suitable model is developed may offer further support to our interpretation. We finally notice that GRB 191019A is not the only burst with long duration detected at low redshift and lacking a supernova component. In all other cases (GRB 060505, Fynbo et al. 2006; GRB 060614, Della Valle et al. 2006; Gal-Yam et al. 2006; Gehrels et al. 2006; GRB 211211A, Mei et al. 2022; Rastinejad et al. 2022; Troja et al. 2022; Yang et al. 2022), however, a clear offset from the

[7] Measurements of the X-ray luminosity function of AGNs in the low-redshift universe (Ueda et al. 2003) show that the low luminosity AGNs ($\sim 10^{41}$–10^{42} erg s^{-1}) are largely outnumbering the high-luminosity ones.

[8] The latter condition can, however, be somewhat relaxed considering the fact that GRB jets can excavate a funnel in the disk and their cocoon emerges (Tagawa et al. 2022).

[9] The former mechanism is dominant in the outer disk regions due to the long alignment times for capture in those regions; see, e.g., Fabj et al. (2020).

host center was detected, making the case of GRB 191019A unique. In addition, the longer of these bursts, GRB 060614 and GRB 211211A, had complex, multipeaked prompt light curves (e.g., Gompertz et al. 2023), different from GRB 191019A. This underlines the fact that there may be multiple mechanisms by which a short-burst engine can produce bursts with prompt gamma-ray emission lasting longer than the canonical 2 s.

Acknowledgments

We would like to acknowledge insightful comments from Daniele Bjørn Malesani and by the anonymous referee that helped to improve the paper. D.L. acknowledges support from NSF grant AST-1907955. R.P. acknowledges support by NSF grant AST-2006839.

Software: Python (https://www.python.org/), emcee (Foreman-Mackey et al. 2013).

ORCID iDs

Davide Lazzati https://orcid.org/0000-0002-9190-662X
Rosalba Perna https://orcid.org/0000-0002-3635-5677
Benjamin P. Gompertz https://orcid.org/0000-0002-5826-0548
Andrew J. Levan https://orcid.org/0000-0001-7821-9369

References

Abbott, B. P., Abbott, R., Abbott, T. D., et al. 2017, ApJL, 848, L12
Abbott, B. P., Abbott, R., Abbott, T. D., et al. 2020a, ApJL, 892, L3
Abbott, R., Abbott, T. D., Abraham, S., et al. 2020b, PhRvL, 125, 101102
Aloy, M. A., Müller, E., Ibáñez, J. M., Martí, J. M., & MacFadyen, A. 2000, ApJL, 531, L119
Artymowicz, P., Lin, D. N. C., & Wampler, E. J. 1993, ApJ, 409, 592
Bellovary, J. M., Mac Low, M.-M., McKernan, B., & Ford, K. E. S. 2016, ApJL, 819, L17
Bromberg, O., & Levinson, A. 2007, ApJ, 671, 678
Callister, T. A., Haster, C.-J., Ng, K. K. Y., Vitale, S., & Farr, W. M. 2021, ApJL, 922, L5
Cantiello, M., Jermyn, A. S., & Lin, D. N. C. 2021, ApJ, 910, 94
Chhotray, A., & Lazzati, D. 2015, ApJ, 802, 132
Della Valle, M., Chincarini, G., Panagia, N., et al. 2006, Natur, 444, 1050
Dittmann, A. J., Cantiello, M., & Jermyn, A. S. 2021, ApJ, 916, 48
Dittmann, A. J., & Miller, M. C. 2020, MNRAS, 493, 3732
Fabj, G., Nasim, S. S., Caban, F., et al. 2020, MNRAS, 499, 2608
Foreman-Mackey, D., Hogg, D. W., Lang, D., & Goodman, J. 2013, PASP, 125, 306
Fynbo, J. P. U., Watson, D., Thöne, C. C., et al. 2006, Natur, 444, 1047
Gal-Yam, A., Fox, D. B., Price, P. A., et al. 2006, Natur, 444, 1053
Gehrels, N., Norris, J. P., Barthelmy, S. D., et al. 2006, Natur, 444, 1044
Ghisellini, G., Haardt, F., & Svensson, R. 1998, MNRAS, 297, 348
Giannios, D. 2006, A&A, 457, 763
Giannios, D., & Spruit, H. C. 2007, A&A, 469, 1
Gompertz, B. P., Ravasio, M. E., Nicholl, M., et al. 2023, NatAs, 7, 67
Goodman, J. 2003, MNRAS, 339, 937
Gottlieb, O., & Nakar, E. 2022, MNRAS, 517, 1640
Gottlieb, O., Nakar, E., & Bromberg, O. 2021, MNRAS, 500, 3511
Hopkins, P. F., Hernquist, L., Hayward, C. C., & Narayanan, D. 2012, MNRAS, 425, 1121
Ito, H., Just, O., Takei, Y., & Nagataki, S. 2021, ApJ, 918, 59
Ito, H., Matsumoto, J., Nagataki, S., Warren, D. C., & Barkov, M. V. 2015, ApJL, 814, L29
Jermyn, A. S., Dittmann, A. J., Cantiello, M., & Perna, R. 2021, ApJ, 914, 105
Kinney, A. L., Schmitt, H. R., Clarke, C. J., et al. 2000, ApJ, 537, 152
Lazzati, D. 2016, ApJ, 829, 76
Lazzati, D., Ciolfi, R., & Perna, R. 2020, ApJ, 898, 59
Lazzati, D., & Perna, R. 2019, ApJ, 881, 89
Lazzati, D., Perna, R., Morsony, B. J., et al. 2018, PhRvL, 120, 241103
Lazzati, D., Soares, G., & Perna, R. 2022, ApJL, 938, L18
Levan, A. J., Malesani, D., Gompertz, B., et al. 2023, NatAs, in press
MacFadyen, A. I., & Woosley, S. E. 1999, ApJ, 524, 262
Matzner, C. D. 2003, MNRAS, 345, 575
McKernan, B., Ford, K. E. S., Callister, T., et al. 2022, MNRAS, 514, 3886
McKernan, B., Ford, K. E. S., & O'Shaughnessy, R. 2020, MNRAS, 498, 4088
Mei, A., Banerjee, B., Oganesyan, G., et al. 2022, Natur, 612, 236
Morsony, B. J., Lazzati, D., & Begelman, M. C. 2007, ApJ, 665, 569
Murguia-Berthier, A., Montes, G., Ramirez-Ruiz, E., De Colle, F., & Lee, W. H. 2014, ApJL, 788, L8
Nagakura, H., Hotokezaka, K., Sekiguchi, Y., Shibata, M., & Ioka, K. 2014, ApJL, 784, L28
Parsotan, T., & Lazzati, D. 2018, ApJ, 853, 8
Pe'er, A., Mészáros, P., & Rees, M. J. 2005, ApJ, 635, 476
Pe'er, A., Mészáros, P., & Rees, M. J. 2006, ApJ, 642, 995
Perna, R., Lazzati, D., & Cantiello, M. 2021a, ApJL, 906, L7
Perna, R., Tagawa, H., Haiman, Z., & Bartos, I. 2021b, ApJ, 915, 10
Piran, T. 2004, RvMP, 76, 1143
Rastinejad, J. C., Gompertz, B. P., Levan, A. J., et al. 2022, Natur, 612, 223
Ray, M., Lazzati, D., & Perna, R. 2023, MNRAS, 521, 4233
Ruiz, M., Lang, R. N., Paschalidis, V., & Shapiro, S. L. 2016, ApJL, 824, L6
Salafia, O. S., Barbieri, C., Ascenzi, S., & Toffano, M. 2020, A&A, 636, A105
Samsing, J., Bartos, I., D'Orazio, D. J., et al. 2022, Natur, 603, 237
Sirko, E., & Goodman, J. 2003, MNRAS, 341, 501
Tagawa, H., Haiman, Z., & Kocsis, B. 2020, ApJ, 898, 25
Tagawa, H., Kimura, S. S., Haiman, Z., et al. 2022, ApJ, 927, 41
Thompson, T. A., Quataert, E., & Murray, N. 2005, ApJ, 630, 167
Troja, E., Fryer, C. L., O'Connor, B., et al. 2022, Natur, 612, 228
Ueda, Y., Akiyama, M., Ohta, K., & Miyaji, T. 2003, ApJ, 598, 886
Wang, Y.-H., Lazzati, D., & Perna, R. 2022, MNRAS, 516, 5935
Wang, Y.-H., McKernan, B., Ford, S., et al. 2021, ApJL, 923, L23
Yang, J., Ai, S., Zhang, B.-B., et al. 2022, Natur, 612, 232
Yang, Y., Gayathri, V., Bartos, I., et al. 2020, ApJL, 901, L34
Zhu, J.-P., Wang, K., & Zhang, B. 2021a, ApJL, 917, L28
Zhu, J.-P., Zhang, B., Yu, Y.-W., & Gao, H. 2021b, ApJL, 906, L11